
ON GLOBAL APPLICABILITY AND LOCATION TRANSFERABILITY OF GENERATIVE DEEP LEARNING MODELS FOR PRECIPITATION DOWNSCALING

Paula Harder
ECMWF & Mila Quebec AI Institute

Christian Lessig, Matthew Chantry
ECMWF

Francis Pelletier, David Rolnick
Mila Quebec AI Institute

ABSTRACT

Deep learning offers promising capabilities for the statistical downscaling of climate and weather forecasts, with generative approaches showing particular success in capturing fine-scale precipitation patterns. However, most existing models are region-specific, and their ability to generalize to unseen geographic areas remains largely unexplored. In this study, we evaluate the generalization performance of generative downscaling models across diverse regions. Using a global framework, we employ ERA5 reanalysis data as predictors and IMERG precipitation estimates at 0.1° resolution as targets. A hierarchical location-based data split enables a systematic assessment of model performance across 15 regions around the world.

Keywords Downscaling · Generative Modeling · Transferability

1 Introduction

Accurate modeling of weather and climate is critical for understanding global climate dynamics and supporting adaptation strategies in sectors such as agriculture, infrastructure, and renewable energy. However, global climate and weather models typically operate at coarse spatial resolutions of 10–80 km, which limits their ability to capture fine-scale processes such as extreme rainfall, topographic effects, and coastal dynamics. High-resolution data are essential not only for assessing the impacts of extreme events but also for optimizing renewable energy production and informing adaptation measures.

Downscaling addresses this limitation by deriving high-resolution information from coarse-resolution model outputs. This is particularly important for precipitation, where rainfall patterns can vary substantially at scales below those resolved by global models. Conceptually, downscaling resembles super-resolution in computer vision, but with important differences: it must correct biases in the input data and often leverages multiple large-scale predictors to estimate fine-scale targets, a process known as heterogeneous downscaling.

A widely used strategy is stochastic downscaling, which generates ensembles of high-resolution realizations consistent with large-scale dynamics while capturing small-scale uncertainties such as terrain influences and coastal effects. Such probabilistic approaches are especially suitable, as the mapping between coarse and fine scales is inherently uncertain and cannot be fully resolved with deterministic models given computational constraints.

The effectiveness of deep learning methods for downscaling is strongly dependent on the availability and distribution of high-quality training data. Although large volumes of climate and weather data exist, observational coverage is geographically imbalanced: often data are scarce in the Global South, for example, ground-based radar precipitation measurements. This imbalance poses challenges for generalization, as precipitation processes vary widely across regions; for example, convection-driven rainfall in equatorial areas differs fundamentally from precipitation regimes in Europe or North America.

In this paper, we investigate the generalization of a generative downscaling model to unseen locations. We focus on precipitation downscaling using an architecture based on Harris et al. [2022]. For global evaluation, we construct a downscaling task from ERA5 predictors at 0.25° resolution to precipitation from the satellite-based IMERG product. The globe is divided into nine subregions, from which we define hierarchical datasets yielding 15 training areas. We analyze if and how model performance degrades when applied outside the training regions, with particular emphasis on the role of changing orography.

2 Related Work

Deep learning is increasingly used for climate and weather downscaling, particularly in probabilistic precipitation downscaling [Rampal et al., 2024]. For a recent overview we refer to Rampal et al. [2024]. Super-resolution CNNs, especially U-Nets [Sha et al., 2020a, Höhle et al., 2020] and ResNets [Liu et al., 2020, Rocha Rodrigues et al., 2018], are among the most common architectures for downscaling. While some standard computer vision models can be directly applied, adaptation is required to address certain Earth system challenges. Recent advancements for specific data types include explainable and interpretable methods [González-Abad et al., 2023, Rampal et al., 2022], physics-constrained neural networks [Harder et al., 2023, Geiss and Hardin, 2020, González-Abad et al., 2023], and arbitrary-resolution downscaling using Fourier neural operators [Yang et al., 2023].

Precipitation downscaling presents unique challenges, particularly in capturing stochastic high-frequency variations. Generative models have been most successful in this regard, with conditional generative adversarial networks (cGANs) [Goodfellow et al., 2014] being a popular choice [Leinonen et al., 2020, Price and Rasp, 2022, Harris et al., 2022], especially stabilized variants like Wasserstein GANs [Harris et al., 2022, Cooper et al., 2023]. More recently, diffusion-based models [Sohl-Dickstein et al., 2015] have demonstrated strong performance in this domain [Mardani et al., 2023, Wan et al., 2023, Addison et al., 2024, Ling et al., 2024], leveraging their ability to model complex distributions.

Generalization across geographies is an active research area in applied ML, particularly in remote sensing and biodiversity modeling. In agricultural classification and segmentation, approaches such as task-informed meta-learning Tseng et al. [2022], versions of model-agnostic meta-learning Rußwurm et al. [2020], and multi-source unsupervised domain adaptation Wang et al. [2022] have shown promise in adapting to new regions with minimal data. In biodiversity monitoring, Teng et al. [2023] integrate remote sensing and citizen science data to improve generalization in data-sparse regions like Kenya, while Cole et al. [2023] leverage spatial implicit neural representations for scalable global species range estimation using noisy, sparse data. However, in Earth system modeling geographical generalization remains underexplored. Initial studies have investigated the regional generalizability of downscaling models Zhu and Zhou [2024]. For instance, some works examine generalization between different areas on the US West Coast Sha et al. [2020a,b]. Others analyze performance across regions in the UK and the United States Cooper et al. [2023] or evaluate generalization from the DACH region (Germany, Austria, and Switzerland) to North America Prasad et al. [2024]. While these efforts provide valuable insights, their geographic scope remains limited. Here, we expand on this by providing the first worldwide evaluation for downscaling transferability.

3 Data

Our dataset combines ERA5 reanalysis data, IMERG satellite precipitation estimates, and high-resolution static geographic fields (orography and land-sea mask). ERA5 serves as the low-resolution (LR) input, while IMERG provides the high-resolution (HR) target for downscaling. The dataset covers nearly the entire globe between 60°N and 60°S — the region of complete IMERG coverage.

3.1 Input: ERA5

ERA5 [Hersbach et al., 2020] is the fifth-generation atmospheric reanalysis produced by the European Centre for Medium-Range Weather Forecasts (ECMWF). Reanalysis datasets combine historical observations with numerical weather prediction models to generate consistent, gridded estimates of the past state of the atmosphere. ERA5 provides hourly global fields at a spatial resolution of $0.25^\circ \times 0.25^\circ$ (approximately 25 km per grid cell at mid-latitudes) on a regular latitude-longitude grid, spanning from 1950 to the present. To align with IMERG availability, we use data from 2001 onward.

Following Harris et al. [2022], originally informed by domain knowledge and the ecPoint model [Hewson and Pilloso, 2020], we select nine predictor variables known to influence precipitation processes. These include precipitation types, atmospheric moisture content, and dynamic fields:

1. Total precipitation (tp)

2. Convective precipitation (cp)
3. Convective available potential energy (cape)
4. Total water content (twc)
5. Total liquid water content (tlwc)
6. Surface pressure (sp)
7. Top-of-atmosphere incident solar radiation (tISR)
8. Eastward wind component at 700 hPa (u)
9. Northward wind component at 700 hPa (v)

3.2 Input: Geographic Features

To provide additional static context, we include two high-resolution (0.1°) geographic fields: (i) a land–sea mask indicating the land fraction within each grid cell, and (ii) an orography map, represented as geopotential height at the surface. These static variables are known to strongly influence local precipitation patterns, especially in regions with complex topography or coastal influences.

3.3 Target: IMERG

The Integrated Multi-satellite Retrievals for GPM (IMERG) product [Huffman et al., 2014] is part of NASA’s Global Precipitation Measurement (GPM) mission. IMERG combines observations from the GPM satellite constellation with additional inputs such as gauge data to produce globally gridded precipitation estimates. It provides near-global coverage between 60°N and 60°S at 0.1° spatial resolution (about 10 km per pixel) and hourly temporal resolution. We use the IMERG V07 Final Run product [Huffman et al., 2024] as the high-resolution target field.

3.4 Preprocessing

Minimal preprocessing is applied to the raw data, which are downloaded directly from publicly available sources. IMERG’s native half-hourly precipitation fields are averaged to hourly resolution to match ERA5. All data are then converted from NetCDF to NumPy array format to improve I/O efficiency during training. Alternative storage formats such as Zarr can be used if metadata retention is required.

Finally, the data are spatially partitioned into nine latitude–longitude subregions, as shown in Figure 1. These subregions are further grouped into larger composite regions: north (N), tropics (T), south (S), west (W), middle (M), east (E), resulting in a total of 15 distinct training domains used in our experiments (see Section 4.5 for details).

4 Methodology

For this work, we adopt the generative adversarial network (GAN) architecture proposed by Harris et al. [2022] and adapt it to our precipitation downscaling task with minor modifications and targeted hyperparameter tuning.

4.1 GAN Overview

Generative Adversarial Networks (GANs) are a class of deep generative models that learn to synthesize data samples resembling a target distribution through a two-player minimax game. A generator network attempts to produce realistic high-resolution samples from low-resolution inputs, while a discriminator learns to distinguish generated outputs from real observations. To improve training stability and address common issues such as mode collapse, we use the Wasserstein GAN (WGAN) formulation [Arjovsky et al., 2017]. WGAN replaces the standard adversarial objective with the Wasserstein distance.

4.2 Model Architecture

We employ the WGAN setup from Harris et al. [2022] with minor adaptations. The training objective consists of three terms: (i) A supervised content loss based on the mean squared error (MSE) between the mean of the generated ensemble and the target field. (ii) An adversarial loss encouraging the generator to produce realistic fine-scale structures. (iii) A gradient penalty term applied to the discriminator to ensure Lipschitz continuity.

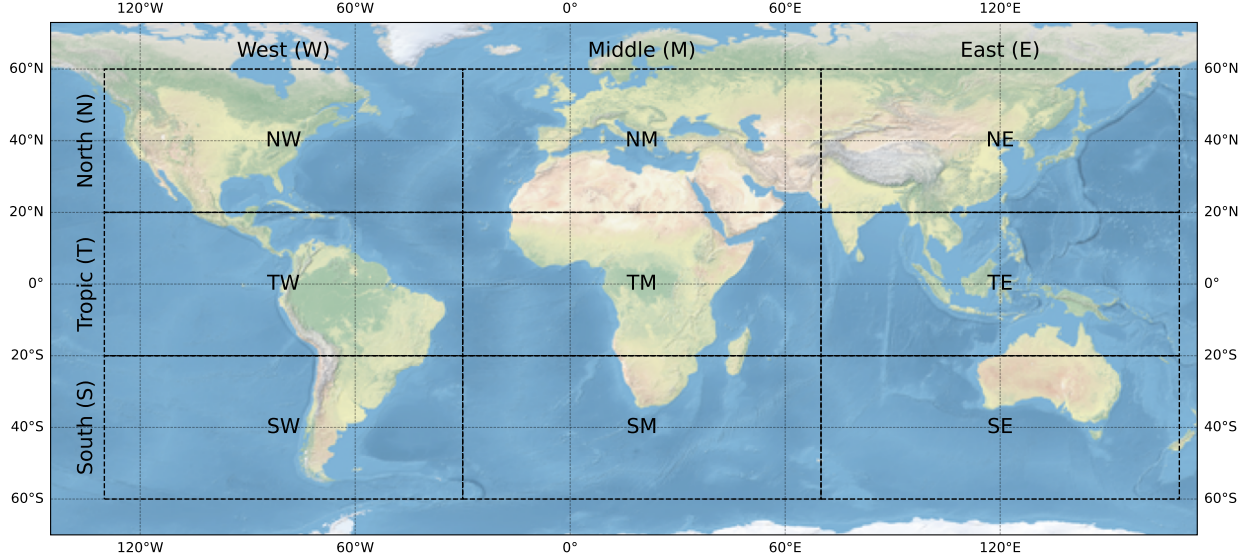


Figure 1: Spatial domain and regional partitioning of the dataset. The covered area extends from 60°N to 60°S and 130°W to 170°E. We first divide the domain into nine rectangular subregions, which are then combined into larger regions (N, T, S, W, M, E) to create 15 training areas in total.

The generator follows a ResNet-style architecture and takes as input the selected ERA5 variables and static geographic features. It outputs high-resolution precipitation fields at 0.1° resolution. The discriminator (critic) receives three inputs — the generated sample, the low-resolution input, and the static fields — and is composed of residual blocks, average pooling layers, and a final dense classification head. Further architectural details can be found in Harris et al. [2022].

Hyperparameters Hyperparameters were selected through a combination of Bayesian optimization using the Weights & Biases framework [Biewald, 2020] and manual fine-tuning. The search was conducted on a reduced-resolution setup (downsampling input and target resolution by a factor of four) to accelerate experimentation. A key finding was that setting the generator learning rate higher than that of the discriminator improved convergence, contrary to the original configuration in Harris et al. [2022]. Final hyperparameters are as follows: generator learning rate = 0.005, discriminator learning rate = 0.0005, content loss weight = 300, gradient penalty weight = 10, and ensemble size for the content loss = 8. Both networks use the Adam optimizer, with 128 filters in the generator and 256 filters in the discriminator.

4.3 Baselines

The superior performance of the WGAN relative to conventional baselines was demonstrated in Harris et al. [2022]. In this study, we include a simple baseline — bilinear interpolation of total ERA5 precipitation — to quantify the relative performance of the downscaling model across regions.

4.4 Training

Each model is trained for five epochs. Given the dataset size, this corresponds to approximately 3–5 days of training on two NVIDIA A100 GPUs using distributed training via the Hugging Face Accelerate framework [Gugger et al., 2022]. Before training, both ERA5 precipitation variables (tp, cp) and IMERG precipitation targets are log-transformed using $\log(x + 10^{-5})$. All variables, including the transformed precipitation fields, are then normalized and standardized using the global mean and standard deviation computed per variable, except for the land–sea mask, which remains unchanged.

4.5 Experiments

As shown in Figure 1, we divide the globe (from 60°N–60°S and 130°W–170°E) into nine equally sized latitude–longitude subregions. These are further combined into larger regions — North (N), Tropics (T), South (S), West (W), Middle (M), and East (E) — resulting in a total of 15 training domains. For each of these 15 regions, we train a separate GAN, which is subsequently evaluated on all nine subregions to assess generalization performance.

We additionally split the data temporally. Training is performed on the years 2001–2018. The years 2019 and 2020 are reserved for validation, hyperparameter tuning, and checkpoint selection. The final evaluation is conducted on 2021–2022 data, from which we compute Continuous Ranked Probability Scores (CRPS).

4.6 Evaluation

Various metrics were investigated in Harris et al. [2022], here we focus on one major metric, the continuous ranked probability score (CRPS). The CRPS is a metric used to evaluate the accuracy of probabilistic forecasts. For a given forecast probability distribution F and the observed outcome y , the CRPS is calculated as follows:

$$\text{CRPS}(F, y) = \int_{-\infty}^{\infty} [F(z) - \mathbf{1}(z \geq y)]^2 dz. \quad (1)$$

Here, $F(z)$ is the cumulative distribution function of the forecast distribution at point z and $\mathbf{1}(\cdot)$ the indicator function. For a deterministic forecast, the CRPS reduces to a mean-average error (MAE).

5 Results and Discussion

Total CRPS Scores The overall CRPS performance across training–evaluation region pairs is shown in Figure 2. We observe substantial variability between evaluation regions, whereas differences between training locations evaluated at the same target location are comparatively minor. This is further illustrated by the leftmost column of Figures 3 and 4, where the rows (corresponding to different training regions) show very similar spatial patterns.

The most challenging evaluation region are consistently in the tropics, which exhibits the highest CRPS scores — likely due to these region’s large precipitation amounts and strong convective activity. Some notable outliers highlight specific transfer difficulties: for example, models trained in the southeastern (Australia) region perform poorly in NE, TW, and SW — areas with complex topography. Similarly, the model trained on the South African region (SE) struggles in NE, which includes the Tibetan Plateau. These cases point to limitations in transferring models from low-relief to high-relief regions, discussed further below.

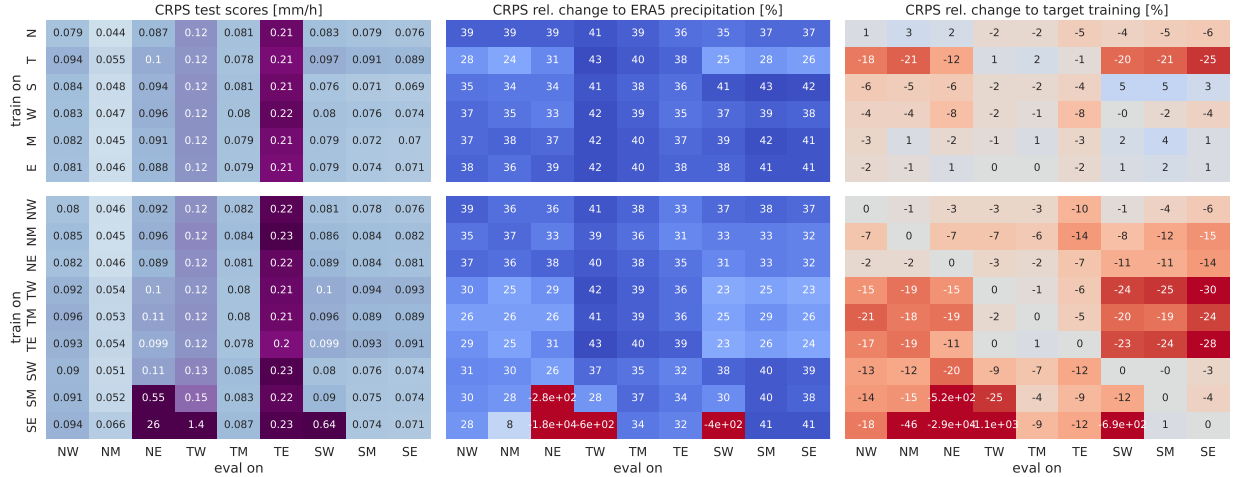


Figure 2: CRPS scores for all training–evaluation region combinations. Rows correspond to training regions, columns to evaluation regions. Lower scores indicate better performance. The left column shows the overall CRPS performance.

CRPS Improvement Over ERA5 Interpolation Compared to bilinear interpolation of ERA5 precipitation, the GAN achieves substantial performance gains in nearly all cases, consistent with findings from Harris et al. [2022]. Except for five outliers, CRPS scores improve by 23–42% relative to the ERA5 baseline (see Figure 2, middle table).

Interestingly, while total CRPS values are lowest in the extratropics, relative improvements are largest in the tropics — particularly over the Atlantic and Pacific oceans (Figure 3, middle column). Improvements are highest along the diagonal (i.e., when training and evaluation regions match), but extending the training region can also mitigate performance drops. For example, including the Sahara in the training domain improves performance in that region, demonstrating the value of broader training coverage.

Performance Relative to Direct Training on the Target The right column of Figure 2 and the rightmost plots in Figure 3 compare model performance to directly training on the target region. As expected, models trained directly on the target achieve the best scores. However, some consistent transferability patterns emerge: models trained in extratropical regions generalize reasonably well to the tropics, whereas the reverse transfer (tropics \rightarrow extratropics) results in larger performance drops.

Interestingly, northern-hemisphere models transfer better to the tropics than southern-hemisphere ones, and vice versa. This is despite the southern and northern extratropics being climatologically more similar to each other than either is to the tropics. Enlarging the training domain to include both the target and surrounding regions also improves performance — with up to a 5% gain observed for the southern region.

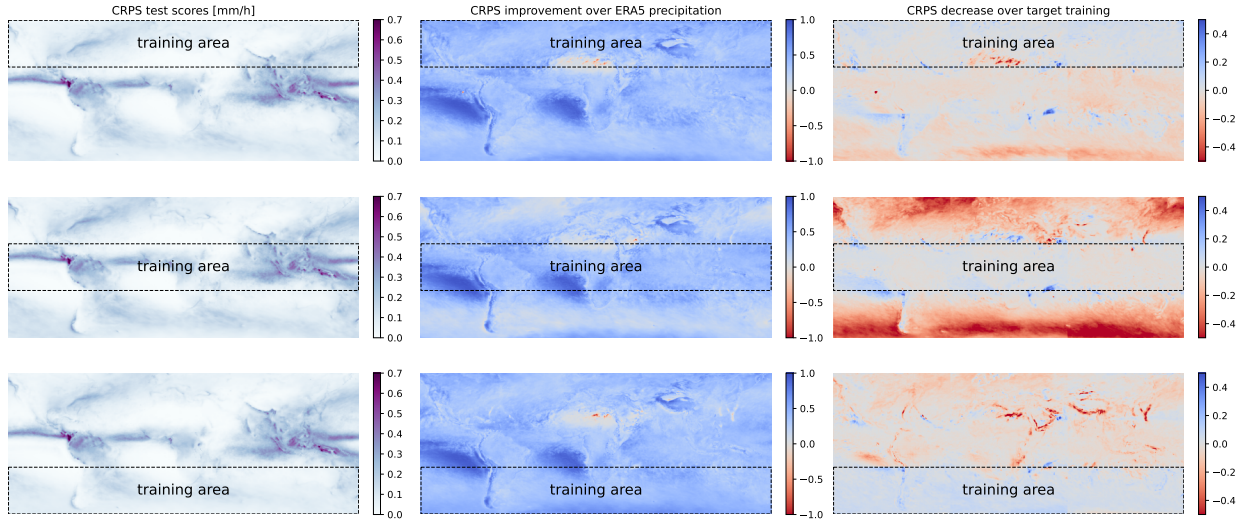


Figure 3: CRPS score maps for three representative training regions: North (N), Tropics (T), and South (S). Left: raw CRPS. Middle: relative improvement over ERA5. Right: relative performance drop compared to direct training on the target region.

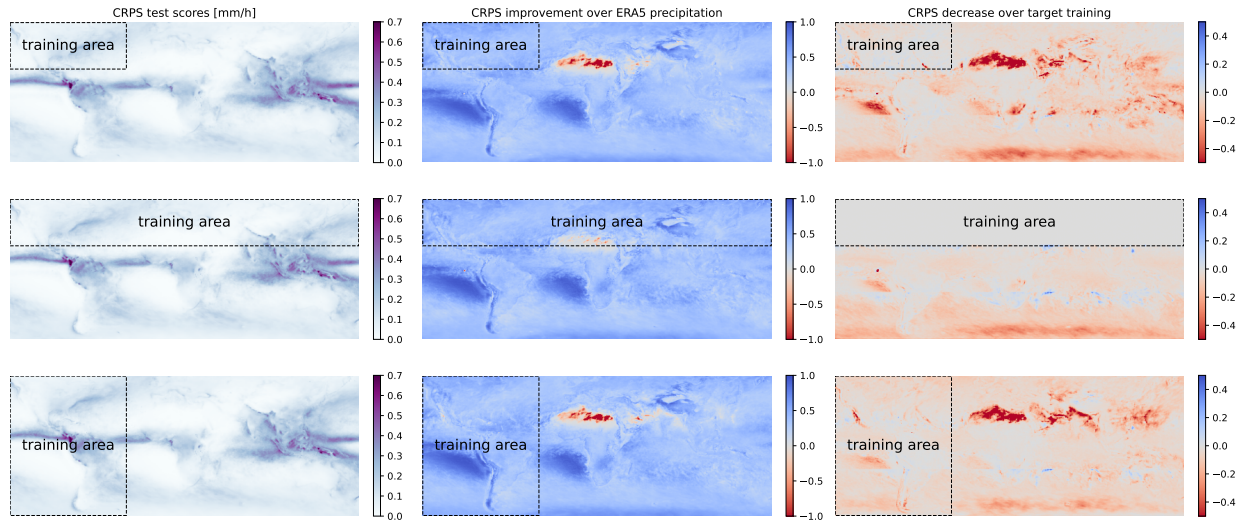


Figure 4: As in Figure 3, but for a hierarchical training setup: starting with Northwest (NW) and progressively enlarging the training domain. Enlarging the domain generally improves transfer performance, especially when the target region is included.

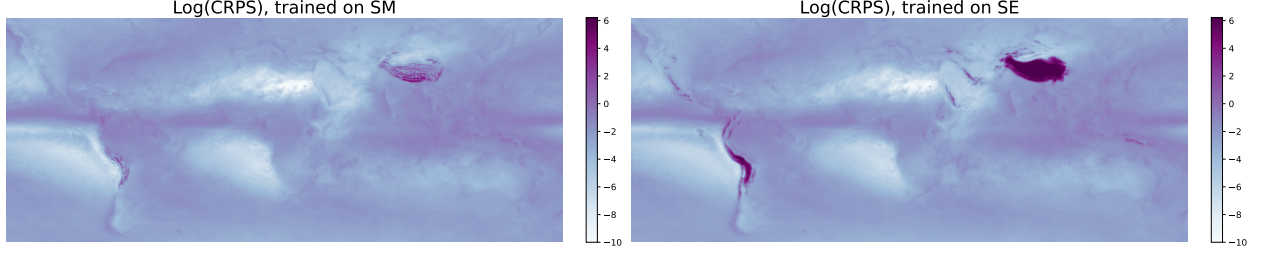


Figure 5: The logarithm of the CRPS score is shown globally, averaged over the whole test period. On the left it shows the performance of the GAN trained on SM on the right trained on SE.

Table 1: Ablation study comparing models trained with and without high-resolution geographic features. CRPS (lower is better) for precipitation [mm/h] is shown for each evaluation region. Values represent the mean pixel-wise CRPS across 8 ensemble members. Best scores are in bold; failures are highlighted in red.

TRAIN AREA	TRAIN GEO	INF. GEO	EVAL AREAS								
			NW	NM	NE	TW	TM	TE	SW	SM	SE
SM	✓	✓	0.091	0.052	0.549	0.146	0.083	0.220	0.090	0.075	0.074
SM	×	×	0.090	0.056	0.126	0.141	0.085	0.247	0.081	0.074	0.072
SE	✓	✓	0.094	0.066	26.0	1.40	0.087	0.227	0.636	0.074	0.071
SE	×	×	0.093	0.053	0.136	0.175	0.084	0.232	0.085	0.075	0.072
NW	✓	✓	0.078	0.046	0.092	0.120	0.082	0.223	0.081	0.078	0.076
NW	×	×	0.081	0.047	0.092	0.124	0.084	0.217	0.085	0.079	0.080

Performance Failures: SM and SE Severe performance degradation occurs when transferring models trained in SM or SE to high-elevation regions (e.g., NE, TW, TE, and SW). Both SM and SE are characterized by low elevation, and their models fail when applied to regions dominated by complex topography. These findings indicate that terrain-related processes, which are not well represented in the training data, pose a significant out-of-distribution challenge. In Figure 6 we see that the very high CRPS values are located in areas like the Himalayas and Andes.

The Role of Orography To better understand the role of static geographic features — here orography and land–sea mask — we conduct ablation experiments in which these inputs are excluded during training and inference (Table 1).

For models trained in low-elevation regions (SM and SE), removing high-resolution geographic features alleviates several model failures (marked in red). This suggests that when the training domain lacks topographic variability it can harm generalization to mountainous regions. For other, less mountainous target areas, including high-res features is not improving performance when training on SE and SM. The only exception is TE, where including the land–sea mask slightly improves performance, likely due to the region’s many islands.

Conversely, for models trained in high-relief regions such as NW, including high-resolution geographic inputs generally improves performance across most evaluation domains. Here, interestingly, TE is the only target area where there are better results without high-res input features.

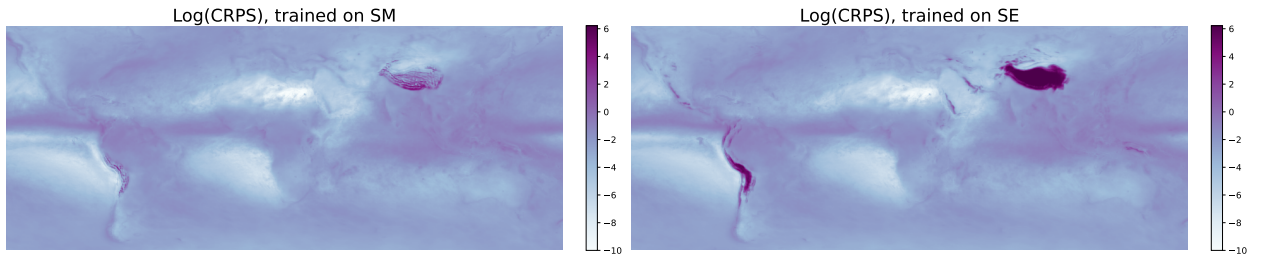


Figure 6: Global CRPS (log scale) averaged over the test period for models trained on SM (left) and SE (right). Strong performance degradation occurs in mountainous regions such as NE and TW.

6 Conclusions

This work demonstrates the successful application of a WGAN-based model to a novel precipitation downscaling task using IMERG as the target. Our results show strong global performance and clear improvements over ERA5 when transferring the model to new locations: in 12 out of 16 cases, the WGAN outperforms the baseline, achieving performance gains of 23–43% in 11 of them. This suggests that machine learning downscaling models can, under certain conditions, be applied beyond their training domains without additional adaptation.

However, performance degradation remains a significant challenge when transferring to unseen regions. In four cases, the model fails entirely, and in others, we observe performance drops of up to 46%, with typical decreases ranging from 3 – 25%. Orography in particular introduces substantial out-of-distribution challenges, indicating that it may be better to exclude regions with largely different topography when deploying models trained elsewhere or dropping topography as a feature. Beyond these low-to-high elevation transitions, the tropics present the most difficult area to transfer from. Models trained on extratropical regions tend to generalize better to tropical climates than the reverse, and those trained in the Northern Hemisphere transfer more effectively to the tropics than those trained in the south.

Further analysis could investigate the temporal distribution of the CRPS to assess whether model performance is dominated by individual events, as suggested by some sharp spatial patterns. Complementary evaluation metrics, especially those targeting extremes, would also provide a more comprehensive understanding of model behavior. Future work could extend this study by exploring alternative architectures, such as diffusion-based models, and by moving beyond ERA5 reanalysis data to IFS hindcasts. Incorporating location-restricted radar observations in place of globally available satellite data could further enhance the relevance and applicability of downscaling approaches.

References

- Henry Addison, Elizabeth Kendon, Suman Ravuri, Laurence Aitchison, and Peter AG Watson. Machine learning emulation of precipitation from km-scale regional climate simulations using a diffusion model, 2024. URL <https://arxiv.org/abs/2407.14158>.
- Martin Arjovsky, Soumith Chintala, and Léon Bottou. Wasserstein generative adversarial networks. In *Proceedings of the 34th International Conference on Machine Learning (ICML)*, volume 70, pages 214–223. PMLR, 2017.
- Lukas Biewald. Experiment tracking with weights and biases. <https://www.wandb.com/>, 2020. Software available from wandb.com.
- Elijah Cole, Grant Van Horn, Christian Lange, Alexander Shepard, Patrick Leary, Pietro Perona, Scott Loarie, and Oisín Mac Aodha. Spatial Implicit Neural Representations for Global-Scale Species Mapping. In *ICML*, 2023.
- Fenwick C. Cooper, Andrew T. T. McRae, Matthew Chantry, Bobby Antonio, and Tim N. Palmer. Further analysis of cgan: A system for generative deep learning post-processing of precipitation, 2023.
- Andrew Geiss and Joseph C. Hardin. Strict enforcement of conservation laws and invertibility in cnn-based super resolution for scientific datasets, 2020.
- Jose González-Abad, Álex Hernández-García, Paula Harder, David Rolnick, and José Manuel Gutiérrez. Multi-variable hard physical constraints for climate model downscaling. In *Proceedings of the AAAI Symposium Series*, volume 2, pages 62–67, 2023.
- Jose González-Abad, Jorge Baño-Medina, and José Manuel Gutiérrez. Using explainability to inform statistical downscaling based on deep learning beyond standard validation approaches. *Journal of Advances in Modeling Earth Systems*, 15(11):e2023MS003641, 2023. doi: <https://doi.org/10.1029/2023MS003641>. URL <https://agupubs.onlinelibrary.wiley.com/doi/abs/10.1029/2023MS003641>. e2023MS003641 2023MS003641.
- Ian J. Goodfellow, Jean Pouget-Abadie, Mehdi Mirza, Bing Xu, David Warde-Farley, Sherjil Ozair, Aaron C. Courville, and Yoshua Bengio. Generative adversarial networks. *Communications of the ACM*, 63:139 – 144, 2014.
- Sylvain Gugger, Lewis Tunstall, Stas Bekman, et al. Accelerate: A simple way to train and use pytorch models with multi-gpu, tpu, mixed-precision, 2022. URL <https://github.com/huggingface/accelerate>.
- Paula Harder, Alex Hernandez-Garcia, Venkatesh Ramesh, Qidong Yang, Prasanna Sattigeri, Daniela Szwarzman, Campbell Watson, and David Rolnick. Hard-constrained deep learning for climate downscaling. *Journal of Machine Learning Research*, 24(365):1–40, 2023.
- Lucy Harris, Andrew T. T. McRae, Matthew Chantry, Peter Dominik Dueben, and Tim N. Palmer. A generative deep learning approach to stochastic downscaling of precipitation forecasts. *Journal of Advances in Modeling Earth Systems*, 14, 2022.

- Hans Hersbach, Bill Bell, Paul Berrisford, Shoji Hirahara, András Horányi, Joaquín Muñoz-Sabater, Julien Nicolas, Carole Peubey, Raluca Radu, Dinand Schepers, Adrian Simmons, Cornel Soci, Saleh Abdalla, Xavier Abellan, Gianpaolo Balsamo, Peter Bechtold, Gionata Biavati, Jean Bidlot, Massimo Bonavita, Giovanna De Chiara, Per Dahlgren, Dick Dee, Michail Diamantakis, Rossana Dragani, Johannes Flemming, Richard Forbes, Manuel Fuentes, Alan Geer, Leo Haimberger, Sean Healy, Robin J. Hogan, Elías Hólm, Marta Janisková, Sarah Keeley, Patrick Laloyaux, Philippe Lopez, Cristina Lupu, Gabor Radnoti, Patricia de Rosnay, Iryna Rozum, Freja Vamborg, Sebastien Villaume, and Jean-Noël Thépaut. The era5 global reanalysis. *Quarterly Journal of the Royal Meteorological Society*, 146(730):1999–2049, 2020. doi: <https://doi.org/10.1002/qj.3803>.
- Tim Hewson and Fatima Maria Pilloso. A low-cost post-processing technique improves weather forecasts around the world. *Communications Earth & Environment*, 2, 2020.
- G. Huffman, D. Bolvin, D. Braithwaite, K. Hsu, R. Joyce, and P. Xie. Integrated Multi-satellitE Retrievals for GPM (IMERG), version 4.4. NASA’s Precipitation Processing Center, 2014. URL <ftp://arthurhou.pps.eosdis.nasa.gov/gpmdata/>. Accessed: 31 March, 2015.
- George J. Huffman, David T. Bolvin, Robert Joyce, Owen A. Kelley, Eric J. Nelkin, Andrea Portier, Erich F. Stocker, Jackson Tan, Daniel C. Watters, and B. Jason West. IMERG V07 Release Notes. <https://gpm.nasa.gov/resources/documents/imerg-v07-release-notes>, 2024. Accessed: 2025-01-26.
- Kevin Höhle, Michael Kern, Timothy Hewson, and Rüdiger Westermann. A comparative study of convolutional neural network models for wind field downscaling. *Meteorological Applications*, 27(6):e1961, 2020. doi: <https://doi.org/10.1002/met.1961>. URL <https://rmets.onlinelibrary.wiley.com/doi/abs/10.1002/met.1961>.
- Jussi Leinonen, Daniele Nerini, and Alexis Berne. Stochastic super-resolution for downscaling time-evolving atmospheric fields with a generative adversarial network. *IEEE Transactions on Geoscience and Remote Sensing*, 59(9): 7211–7223, 2020.
- F. Ling, Z. Lu, J. J. Luo, et al. Diffusion model-based probabilistic downscaling for 180-year East Asian climate reconstruction. *npj Climate and Atmospheric Science*, 7:131, 2024. doi: 10.1038/s41612-024-00679-1. URL <https://doi.org/10.1038/s41612-024-00679-1>.
- Yumin Liu, Auroop R. Ganguly, and Jennifer Dy. Climate downscaling using ynet: A deep convolutional network with skip connections and fusion. In *Proceedings of the 26th ACM SIGKDD International Conference on Knowledge Discovery & Data Mining, KDD ’20*, page 3145–3153, New York, NY, USA, 2020. Association for Computing Machinery. ISBN 9781450379984. doi: 10.1145/3394486.3403366. URL <https://doi.org/10.1145/3394486.3403366>.
- Morteza Mardani, Noah Brenowitz, Yair Cohen, Jaideep Pathak, Chieh-Yu Chen, Cheng-Chin Liu, Arash Vahdat, Karthik Kashinath, Jan Kautz, and Michael S. Pritchard. Generative residual diffusion modeling for km-scale atmospheric downscaling. *ArXiv*, abs/2309.15214, 2023.
- Ayush Prasad, Paula Harder, Qidong Yang, Prasanna Sattigeri, Daniela Szwarcman, Campbell Watson, and David Rolnick. Evaluating the transferability potential of deep learning models for climate downscaling, 2024.
- Ilan Price and Stephan Rasp. Increasing the accuracy and resolution of precipitation forecasts using deep generative models, 2022. URL <https://arxiv.org/abs/2203.12297>.
- Neelesh Rampal, Peter B. Gibson, Abha Sood, Stephen Stuart, Nicolas C. Fauchereau, Chris Brandolino, Ben Noll, and Tristan Meyers. High-resolution downscaling with interpretable deep learning: Rainfall extremes over new zealand. *Weather and Climate Extremes*, 38:100525, 2022. ISSN 2212-0947. doi: <https://doi.org/10.1016/j.wace.2022.100525>. URL <https://www.sciencedirect.com/science/article/pii/S2212094722001049>.
- Neelesh Rampal, Sanaa Hobeichi, Peter B. Gibson, Jorge Baño-Medina, Gab Abramowitz, Tom Beucier, Jose González-Abad, William Chapman, Paula Harder, and José Manuel Gutiérrez. Enhancing regional climate downscaling through advances in machine learning. *Artificial Intelligence for the Earth Systems*, 2024. doi: 10.1175/AIES-D-23-0066.1.
- Eduardo Rocha Rodrigues, Igor Oliveira, Renato Cunha, and Marco Netto. Deepdownscale: A deep learning strategy for high-resolution weather forecast. In *2018 IEEE 14th International Conference on e-Science (e-Science)*, pages 415–422, 2018. doi: 10.1109/eScience.2018.00130.
- Marc Rußwurm, Sherrie Wang, Marco Körner, and David Lobell. Meta-learning for few-shot land cover classification. *Preprint arXiv 2004.13390*, 2020.
- Yingkai Sha, David John Gagne, Gregory West, and Roland Stull. Deep-learning-based gridded downscaling of surface meteorological variables in complex terrain. part i: Daily maximum and minimum 2-m temperature. *Journal of Applied Meteorology and Climatology*, 2020a.

- Yingkai Sha, David John Gagne II, Gregory West, and Roland Stull. Deep-learning-based gridded downscaling of surface meteorological variables in complex terrain. part ii: Daily precipitation. *Journal of Applied Meteorology and Climatology*, 59(12):2075 – 2092, 2020b. doi: 10.1175/JAMC-D-20-0058.1. URL <https://journals.ametsoc.org/view/journals/apme/59/12/jamc-d-20-0058.1.xml>.
- Jascha Narain Sohl-Dickstein, Eric A. Weiss, Niru Maheswaranathan, and Surya Ganguli. Deep unsupervised learning using nonequilibrium thermodynamics. *ArXiv*, abs/1503.03585, 2015.
- Mélisande Teng, Amna Elmustafa, Benjamin Akera, Yoshua Bengio, Hager Radi, Hugo Larochelle, and David Rolnick. Satbird: a dataset for bird species distribution modeling using remote sensing and citizen science data. In A. Oh, T. Neumann, A. Globerson, K. Saenko, M. Hardt, and S. Levine, editors, *Advances in Neural Information Processing Systems*, volume 36, pages 75925–75950. Curran Associates, Inc., 2023. URL https://proceedings.neurips.cc/paper_files/paper/2023/file/ef7653bbc4655305efb89a32362e332a-Paper-Datasets_and_Benchmarks.pdf.
- Gabriel Tseng, Hannah Kerner, and David Rolnick. Timl: Task-informed meta-learning for agriculture, 2022. URL <https://arxiv.org/abs/2202.02124>.
- Zhong Yi Wan, Ricardo Baptista, Yi-Fan Chen, John R. Anderson, Anudhyan Boral, Fei Sha, and Leonardo Zepeda-Núñez. Debias coarsely, sample conditionally: Statistical downscaling through optimal transport and probabilistic diffusion models. *ArXiv*, abs/2305.15618, 2023.
- Yumiao Wang, Luwei Feng, Weiwei Sun, Zhou Zhang, Hanyu Zhang, Yang Gang, and Meng Xiangchao. Exploring the potential of multi-source unsupervised domain adaptation in crop mapping using sentinel-2 images. *GIScience & Remote Sensing*, 59(1):2247–2265, 2022. doi: 10.1080/15481603.2022.2156123. URL <https://doi.org/10.1080/15481603.2022.2156123>.
- Qidong Yang, Paula Harder, Venkatesh Ramesh, Alex Hernandez-Garcia, Daniela Szwarzman, Prasanna Sattigeri, Campbell D Watson, and David Rolnick. Fourier neural operators for arbitrary resolution climate data downscaling. In *ICLR 2023 Workshop on Tackling Climate Change with Machine Learning*, 2023.
- Honglin Zhu and Qiming Zhou. Advancing satellite-derived precipitation downscaling in data-sparse area through deep transfer learning. *IEEE Transactions on Geoscience and Remote Sensing*, 62:1–13, 2024. doi: 10.1109/TGRS.2024.3367332.